Spike-in enhanced phosphoproteomics uncovers synergistic signaling responses to MEK inhibition in colon cancer cells

Mirjam van Bentum[1,2], Bertram Klinger[2,4], Anja Sieber[2,4], Nadine Lehmann[4], Sheyda Naghiloo[1], Mohamed Haji[1], Sylvia Niquet[1,3], Philipp Mertins[1,3], Nils Blüthgen[2,4]*, Matthias Selbach[1,4]*

[1] Max Delbrück Center for Molecular Medicine, Robert-Rössle-Str. 10, 13092 Berlin, Germany

[2] Faculty of Life Sciences, Humboldt-Universität zu Berlin, Unter den Linden 6, 10117 Berlin, Germany

[3] Berlin Institute of Health, Berlin, Germany

[4] Charité-Universitätsmedizin Berlin, Charitéplatz 1, 10117 Berlin, Germany

Corresponding authors:

Nils Blüthgen
Faculty of Life Sciences, Humboldt-Universität zu Berlin
Unter den Linden 6, D-10117 Berlin, Germany
email: nils.bluethgen@charite.de

Matthias Selbach
Max Delbrück Center for Molecular Medicine
Robert-Rössle-Str. 10, D-13092 Berlin, Germany
email: matthias.selbach@mdc-berlin.de

Abstract

Targeted kinase inhibitors are a cornerstone of cancer therapy, but their success is often hindered by the complexity of cellular signaling networks that can lead to resistance. Overcoming this challenge necessitates a deep understanding of cellular signaling responses. While standard global phosphoproteomics offers extensive insights, lengthy processing times, the complexity of data interpretation, and frequent omission of crucial phosphorylation sites limit its utility. Here, we combine data-independent acquisition (DIA) with spike-in of synthetic heavy stable isotope-labeled phosphopeptides to facilitate the targeted detection of particularly informative phosphorylation sites. Our spike-in enhanced detection in DIA (SPIED-DIA) approach integrates the improved sensitivity of spike-in-based targeted detection with the discovery potential of global phosphoproteomics into a simple workflow. We employed this method to investigate synergistic signaling responses in colorectal cancer cell lines following MEK inhibition. Our findings highlight that combining MEK inhibition with growth factor stimulation synergistically activates JNK signaling in HCT116 cells. This synergy emphasizes the therapeutic potential of concurrently targeting MEK and JNK pathways, as evidenced by the significantly impaired growth of HCT116 cells when treated with both inhibitors. Our results demonstrate that SPIED-DIA effectively identifies synergistic signaling responses in colorectal cancer cells, presenting a valuable tool for uncovering new therapeutic targets and strategies in cancer treatment.

Introduction

Cell signaling plays a key role in human health and disease, and sustained proliferative signaling is recognized as a hallmark of cancer [1]. Correspondingly, kinase inhibitors have established their crucial role in the arsenal of cancer therapy, demonstrating significant efficacy in targeting these proliferative pathways [2,3]. However, cellular responses to targeted therapies are often complicated by resistance mechanisms. Primary resistance to targeted treatment can be caused by feedback mechanisms that lead to rewiring or reactivation of signaling pathways. For example, resistance to PI3K/mTOR inhibition in breast cancer is frequently due to feedback mechanisms that cause activation of JAK/STAT signaling [4]. In neuroblastoma, resistance to Mitogen-Activated Protein Kinase Kinase (MEK) inhibitors can emerge from negative feedback mechanisms within the MAPK signaling and via the IGF receptor, thereby reactivating MAPK signaling upon treatment [5]. In colorectal cancer (CRC), therapy targeting the MAPK pathway is undermined by a negative feedback loop, which results in increased sensitivity of the EGF receptor and consequently leads to the reactivation of both MAPK and AKT signaling pathways [6,7]. These studies collectively emphasize the importance of characterizing cell signaling to predict the outcome of targeted treatment.

Genomic and transcriptomic markers often cannot predict cell line specific resistance to targeted therapy, highlighting the need for alternative methods to characterize cell signaling [5,8,9]. Mass spectrometry-based phosphoproteomics is arguably the best available technology to comprehensively characterize cellular signaling states [10–12]. However, some kinases and phosphorylation sites particularly informative about critical cellular signaling states are low abundant, requiring considerable phosphoproteomics depth to enable their detection. In addition, correct biological interpretation of phosphoproteomic data hinges on the precise and accurate quantification of identified phosphopeptides.

Classical global phosphoproteomics using data dependent acquisition (DDA) can routinely identify thousands of phosphorylation sites in a single sample, with more than 200,000 human phosphorylation sites being mapped in total [13–15]. To attain adequate coverage, DDA global phosphoproteomics relies on extensive fractionation, resulting in long data acquisition times. Despite these efforts, specific phosphorylation sites of interest can still remain undetected. Data independent acquisition (DIA) has emerged as an attractive alternative to classical DDA due to greater proteome coverage of single shot analyses, significantly increasing throughput [16,17]. In combination with ion mobility-based peptide fractionation in the gas phase (diaPASEF), this also results in higher sensitivity [18]. DIA has also been applied to phosphoproteomics [19–22]. However, the number of unique

phosphorylation sites identified by single shot DIA phosphoproteomics is typically lower than in classical global DDA phosphoproteomics, aggravating the problem of missing specific phosphosites of interest [23]. Additionally, due to the highly complex spectra of DIA runs, false discovery control remains an ongoing point of discussion.

An attractive alternative to global phosphoproteomics is the targeted detection of a limited set of key phosphorylation sites reflecting critical kinases and substrates pivotal to cell signaling. Indeed, targeted (phospho-)proteomics approaches such as selected reaction monitoring (SRM) and parallel reaction monitoring (PRM) enable fast, sensitive, and reproducible detection of target peptides and have been successfully applied to study signaling [24,25]. More recently, a number of advanced targeted acquisition methods have been described that employ more sophisticated acquisition strategies to increase the efficiency of mass spectrometers in detecting target peptides [26]. For example, spike-in triggered acquisition methods enabled targeted detection of several hundred tyrosine phosphorylated peptides commonly dysregulated in cancer [27]. While these methods significantly enhance the sensitivity and consistency of target phosphopeptide detection, they demand extensive method development for each target peptide and often involve partly manual data analysis, which can be time-consuming. This complexity limits their practicality for high-throughput experiments. Additionally, while targeted approaches offer precise detection of specific phosphopeptides, they inherently limit the broader discovery potential that is a hallmark of global DDA and DIA phosphoproteomics. Recently, DIA was combined with spike-in triggered acquisition, enabling integrated targeted and DIA-based discovery phosphoproteomics [28]. However, this workflow also requires extensive method optimization and is only available on specific mass spectrometers.

Adding an excess of a heavy stable isotope-labeled reference has been shown to increase sensitivity in DIA [29–31]. The use of heavy stable-isotope labeled synthetic spike-in peptides is also well-established in targeted proteomics and has been shown to increase confidence in target identification and the accuracy of quantification [32–34]. Here, we combined these two concepts to develop *spike-in enhanced detection in DIA* (SPIED-DIA) as a simple and generic method to improve detection of key phosphopeptides in DIA phosphoproteomics. To this end, we synthesized a custom set of heavy stable isotope-labeled phosphopeptides covering a wide range of signaling pathways. Spiking-in this heavy stable isotope labeled reference set improves detection and quantification of key target phosphorylation sites up to three fold. At the same time, the method takes full advantage of the discovery potential of conventional DIA. Applying SPIED-DIA to CRC cells revealed that MEK inhibition stimulates growth factor-induced JNK signaling in HCT116 cells. Consistently, we observed that combinatorial treatment of this cell line with MEK and JNK inhibitors synergistically impairs growth. Hence, phosphorylation-based signaling

responses revealed by SPIED-DIA identify effective drug combinations that overcome primary resistance.

Results

Spike-in enhanced detection improves sensitivity of DIA phosphoproteomics

Heavy stable isotope-labeled synthetic peptides are widely used for targeted (phospho-)proteomics. However, currently available methods either require extensive optimization of acquisition methods, SRM or PRM [26], or complex DDA methods, spike-in triggered acquisition methods such as TOMAHAQ or Surequant [27,35]. We hypothesized that combining a heavy stable isotope-labeled spike-in with standard DIA could leverage the simplicity of DIA along with the enhanced sensitivity provided by the heavy spike-in (Fig. 1 A). Specifically, spiking-in a set of heavy synthetic phosphopeptides into a complex proteome sample would both generate (i) global untargeted phosphoproteomic data and (ii) improve coverage of the targeted phosphopeptides. The increased sensitivity for targeted phosphopeptides is based on the idea that the heavy spike-in peptides serve as beacons facilitating the detection of corresponding endogenous, light, phosphopeptides: While low abundant endogenous phosphopeptides might escape detection, their more abundant synthetic heavy peptide counterpart spiked-in in excess are more readily detectable. This enables identification of the correct retention time and ion mobility of the corresponding light endogenous counterpart, facilitating its detection (Fig. 1 B). Additionally, the same heavy peptides spiked into different samples serves as an internal reference improving across-sample quantification (by computing the ratio of the within sample light to heavy ratios). Hence, spike-in peptides serve a dual purpose: improvement of detection rate and quantitative performance.

We tested this idea by measuring the global phosphoproteome of mixed heavy (H) and light (L) HCT116 cell lysates generated using stable isotope labeling with amino acids in cell culture (SILAC)[36] in serial dilution (Fig. 1 C). Following phosphopeptide enrichment, samples were measured on a timsTOF Pro2 mass spectrometer in triplicates before being processed with DIA-NN[16,17,29] to identify 12,621 unique phosphorylation sites. These data were first analyzed using the standard workflow (normal SILAC-DIA). Detected median peptide ratios were close to expected values, indicating accurate quantification (Fig. 1 D). As expected, we observed a rapid reduction in the number of quantifiable precursor ratios throughout the dilution series, with essentially no target precursors detected at 1:63 dilution or higher. Next we took advantage of the reference peptides as beacons to facilitate detection of target peptides, whereby only confident identification of phosphopeptides in the reference channel was required, relaxing precursor confidence threshold for the target

channel (see Material and Methods for details). For each precursor that passed the combined confidence threshold, we extracted intensities in the target channel. Similar to "requantify" in MaxQuant[37], "RefQuant" for dimethyl labeling[30] and the "requantify" option in DIA spike-in SILAC [31], this spike-in enhanced detection approach conceptually uncouples detection and quantification. In this way, it provides intensity information for target channel precursors that would otherwise escape detection.

We found that spike-in enhanced detection greatly increased the number of quantifiable phosphopeptides in the target channel even at high dilutions (Fig. 1 D). As expected, the data obtained in this manner showed a greater spread (lower precision) and signs of systematic ratio compression at higher dilutions (lower accuracy). To investigate this further, we binned precursors by their intensities and plotted observed SILAC ratios as a function of the dilution series (Fig. 1 E). While precursors with high intensities accurately reflected the expected ratios up to a dilution of 1:255, low intensity precursors started to saturate at dilutions of 1:15. Importantly, despite this ratio compression, the observed ratios consistently showed the correct trend. We also compared SILAC ratios for precursors quantified in both the standard and the SPIED-DIA workflow and observed high consistency (Fig. S1A). In conclusion, precursors identified by both the standard and the SPIED-DIA workflow generated similar ratios. However, SPIED-DIA markedly improved coverage, revealing many additional ratios with varying degrees of ratio compression.

Since peptides with more than one serine, threonine and tyrosine residue can be phosphorylated at different positions, we also tested the quality of phosphorylation site localisation. To this end, we compared H/L ratios for identical heavy and light pairs (that is, peptides phosphorylated on the same amino acid), and positional isomers (that is, peptides with identical amino acid sequence but phosphorylated at different sites). We observed higher precision for pairs than for isomers, especially when filtering for post-translational modification (PTM) site confidence, indicating that DIA-NN accurately localises phosphorylation sites (Fig. S1B,D). We further assessed phospho-site localisation by validating the localisation in spectra from raw files (Fig S4),

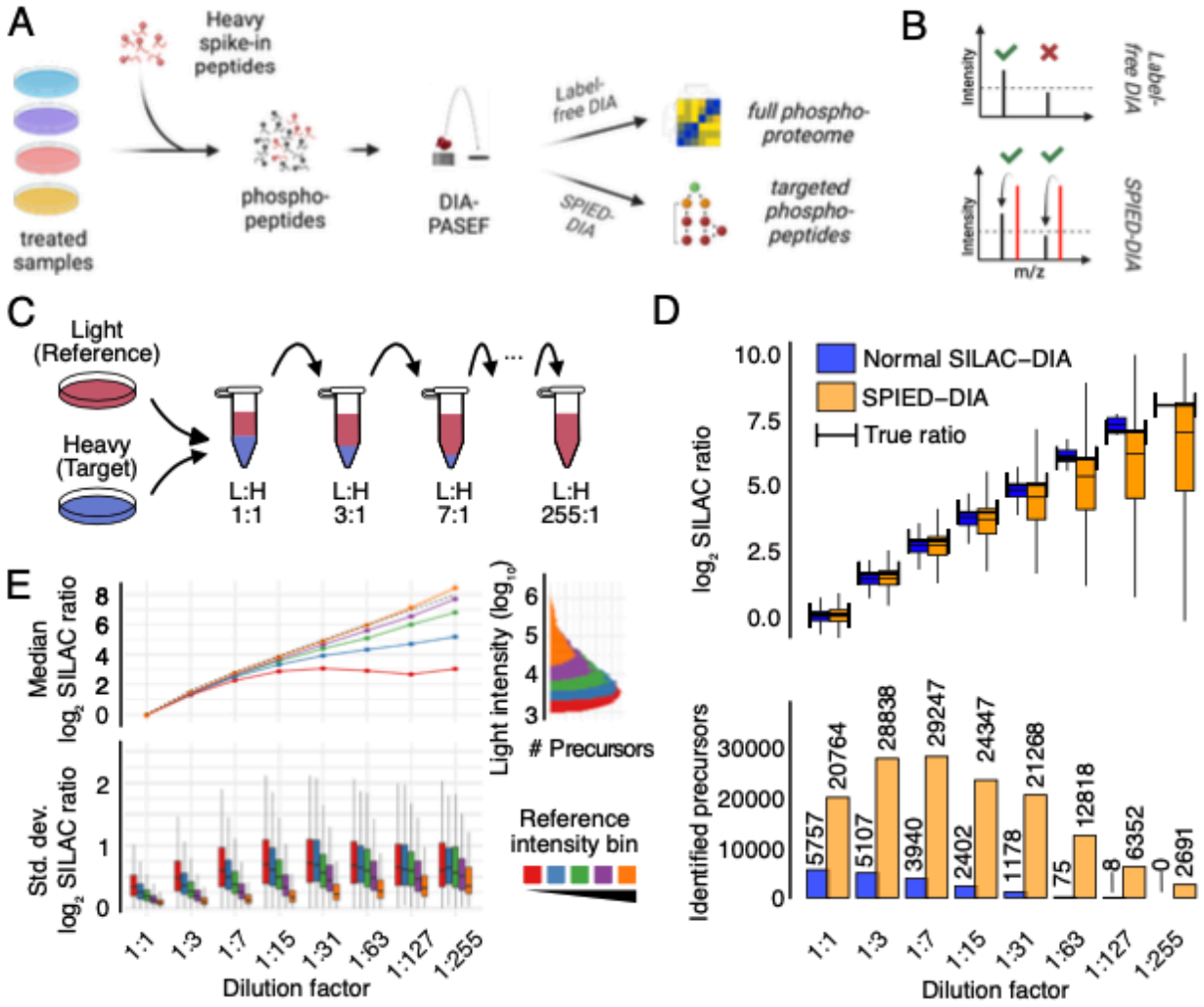

Figure 1: Spike-in enhanced detection in data independent acquisition (SPIED-DIA) (previous page) A. Workflow depicting the integration of Label-free (LF) DIA with SPIED-DIA. B. Quantification and identification in LF-DIA and SPIED-DIA. C. Schematic of the dilution series used to benchmark the performance of SPIED-DIA. D. Number of precursors identified in at least 2 replicates and corresponding H/L channel intensities, n is total IDs in replicates. E. SILAC ratio variability by light intensity and dilution. Lines show median log2 SILAC ratios across dilution factors, binned by reference channel (L) intensity with equally sized bins. Expected ratios are shown as a dotted line. Histogram depicts precursor count distribution by log10 light intensity. Boxplots show standard deviation of log2 SILAC ratios by dilution and bin, aggregated at the modified sequence level. F. Signaling pathway origins of phosphosites selected for spike-in peptide library. G. Improved target peptide identification with SPIED-DIA. Targets identified in 2 out 3 biological replicates, with a CV lower than 10%. Upset plot depicts intersections > 1. wMBR: with match-between-runs, HpH-lib: library created by high pH fractionation phosphoproteomics. H. Dilution series of heavy peptides in light background samples. Relative intensity of dilutions normalised to 500ng L condition, filtered as in panel G.

A Synthetic phosphopeptide panel to study cell signaling

Encouraged by these results, we sought to apply spike-in enhanced detection to study cell signaling. Specifically, we reasoned that spiking-in a selected set of synthetic heavy stable isotope-labeled phosphopeptides would facilitate detection of their endogenous, light, counterparts. To this end, we selected a panel of phosphosites informative for the activity of a wide range of biologically relevant signaling pathways either manually or based on the PhosphositePlus database (Fig. 1F). From the PhosphoSitePlus database, we selected phosphosites that either had known annotated kinases, influenced enzymatic activity or were present on proteins part of selected KEGG signaling pathways. Selected sites were mapped to an *in silico* tryptic digest of the human proteome and peptides meeting criteria for synthesis were ordered. Of the ordered peptides, 206 unique phosphopeptides mapping to 136 proteins were consistently detected (103 pTyr, 26 pThr, 77 pSer peptides). The list of initially selected peptides and peptides consistently detected can be found in Supplemental table 1.

Next, we added our heavy synthetic phosphopeptide panel to HEK293 cell lysate, performed phosphopeptide enrichment and measured samples using DIA-PASEF. To investigate the gain in coverage of targeted sites, we compared our method to conventional label-free quantification without the spike-in (Fig. 1G, S1E). For the label-free analysis we tested both an *in silico* predicted spectral library and an empirically determined library obtained from DIA analysis of deeply high-pH HPLC fractionated phosphopeptide samples (see Materials and Methods for details). For the heavy spike-in samples we generated a library by single shot DDA analyses of the heavy spike-in alone (see Materials and Methods

for details). Comparing both workflows, we observed a significant increase in identified target peptides from 12-24 identified targets to 40 identified target phosphosites, while maintaining a false positive rate of 5%, i.e, 2 targets (Fig. 1G). This increase was not only the result of increased sensitivity from the spike-in but also from the ability to use the smaller empirical phosphopeptide library for the search. Using this library for the sample without the spike-in did not yield any identifications (data not shown). Hence, the increased coverage depends on both the library and the increased sensitivity of spike-in enhanced detection.

Next, we looked at the quantitative performance of SPIED-DIA for the panel of selected phosphosites. To this end, we spiked the same amount of heavy synthetic peptides into decreasing amounts of light phosphopeptides (Fig. 1H). We observed good accuracy and precision throughout the dilution series, as well as a slight loss of target phosphopeptides at higher dilutions (Fig. 1I), consistent with the global data (Fig. 1 D, E). We conclude that SPIED-DIA increases identification of target peptides, maintaining good accuracy and precision.

A screen for synergistic signaling responses in 11 CRC cell lines

Intrinsic resistance of cancer cells to targeted therapies is a significant therapeutic challenge. One known mechanism involves negative feedback from signaling pathways to upstream receptors. Inhibiting a pathway can disrupt this feedback, causing (hyper-)activation of upstream receptors that subsequently activate parallel signaling pathways. In colorectal cancer, we and others observed that inhibiting Mitogen-Activated Protein Kinase Kinase (MEK) rapidly activates the epidermal growth factor receptor (EGFR), which synergistically enhances AKT signaling [6,7].

To more systematically investigate CRC cell responses to MEK inhibition, we initially conducted a screen across a panel of 11 cell lines. We stimulated cells with seven different growth factors or serum, both with and without the MEK inhibitor (MEKi) Selumetinib (AZD6244), and monitored AKT activation using specific antibodies (Fig. 2A). In this experiment, synergistic signaling was defined as an increase in AKT activation caused by growth factors when MEK was inhibited, meaning that the MEKi enhances growth factor-induced AKT activation (Fig. 2B). In addition to confirming the known synergy with EGF, we found that MEK inhibition also led to synergistic AKT activation via FGF2 and VEGF-C in a subset of cells (Fig. 2C, S2). Notably, the two mutant KRAS cell lines, HCT116 and DLD1, exhibited marked synergistic responses while the KRAS wild-type cell line CaCo-2 did not display a notable increase in AKT activation in response to any of the growth

factors (Fig. 2C, 2D). We therefore selected these three cell lines for more detailed analysis via SPIED-DIA.

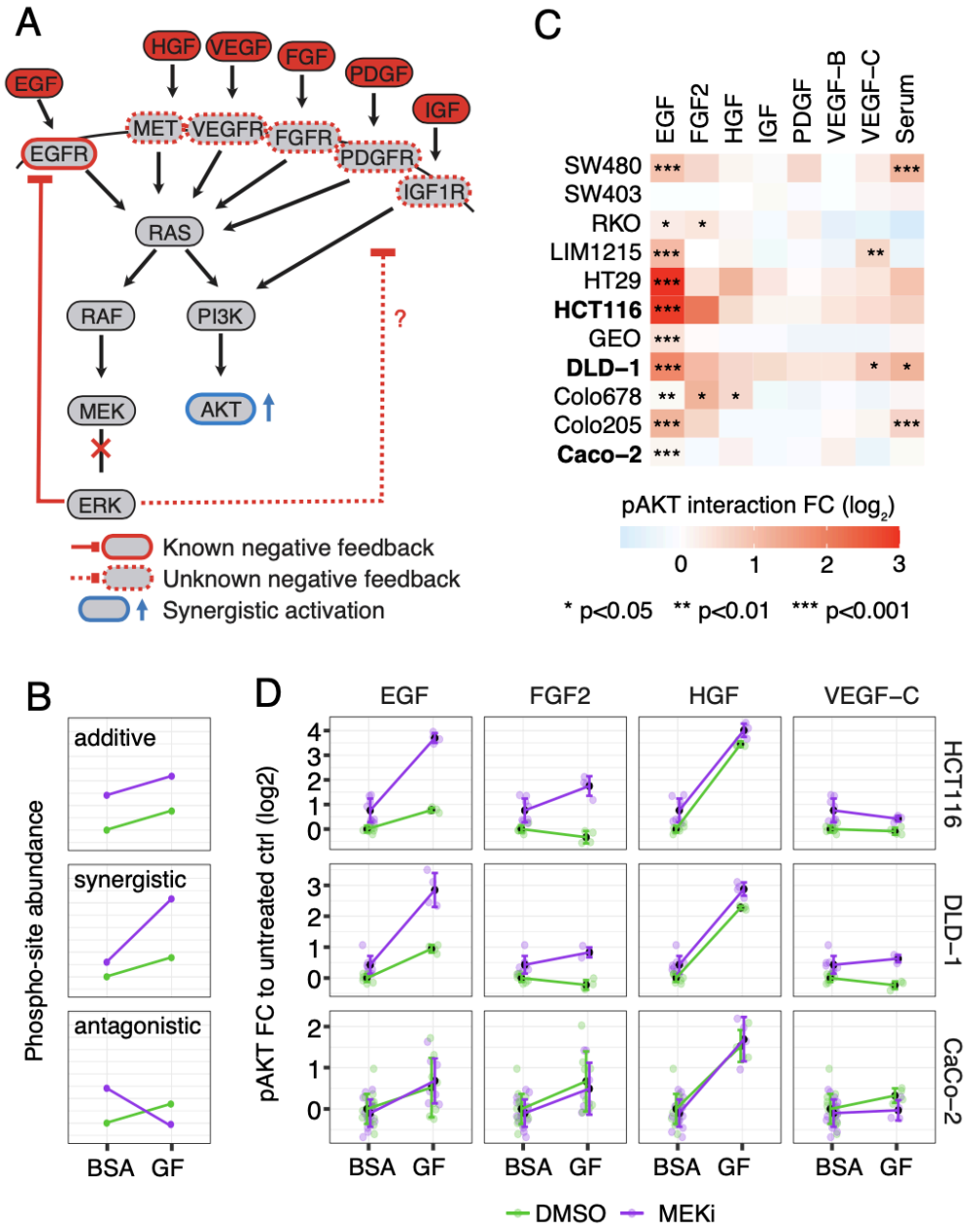

Figure 2: Overview analysis CRC cell-line panel treated with MEKi and growth factor mix. A. Conceptual illustration of synergistic activation of AKT upon MEKi through receptor feedback loops and B. schematic explanation of interaction types. Where possible, color coding was consistent throughout the manuscript. C. Heatmap summarizing screening results for pAKT synergistic activation across CRC cell lines upon 3.5h MEK inhibition and subsequent 30 min stimulation with the indicated growth factors/serum, n ≥ 4. D. Quantitative Luminex measurement of pAKT response to growth factors in CRC cell lines, data are shown as mean ± standard deviation.

Targeted phosphoproteomics of synergistic signaling responses in HCT116, DLD1 and CaCo-2 CRC cells

To uncover additional pathways that could contribute to intrinsic resistance through synergistic activation in CRC, we focused on HCT116, DLD1, and CaCo-2 cells for in-depth phosphoproteomic analysis via SPIED-DIA. Cell lines were treated with either MEKi or DMSO control for 3.5 hours, followed by 30 minute exposure to a growth factor cocktail (EGF, HGF, FGF2, and VEGF-C) or BSA control (Fig. 3A). Cells were subsequently harvested and analyzed using our established workflow. In the global phosphoproteome data we identified 6,000 to 8,000 confidently localised phosphorylation sites per sample (Fig. 3B). SPIED led to a two to threefold increase in the number of identified target phosphopeptides, surpassing the results from a parallel label-free analysis (Fig. 3B).

Principal Component Analysis (PCA) of the global phosphoproteomic data across all cell lines showed that cell line identity was the primary factor driving differences (Fig. 3C), confirming prior research[8]. We therefore conducted PCA on each individual cell line (Fig. 3D) to evaluate the impact of treatment. Interestingly, responses reflected the mutational profile of the cell lines. For instance, HCT116, characterized by oncogenic mutations including $KRAS^{G13D}$, $PIK3CA^{H1047R}$, $CTNNB1^{S45del}$ [38,39], exhibited a noticeable shift in its phosphoproteome along the first principal component (PC1) following MEKi treatment, with the second principal component (PC2) showing the response to the growth factor mix. Similarly, DLD-1, which has a mutational profile that includes $KRAS^{G13D}$, $PIK3CA^{E545K}$ and $PIK3CA^{D549N}$ mutations and APC truncation [40], displayed treatment responses that clustered closely together. CaCo-2, lacking mutations in RAS/RAF/PIK3CA, showed no phosphoproteomic shift with MEKi treatment alone. However, adding the growth factor mix caused a significant change that was largely mitigated when combined with MEKi treatment.

To further understand signaling responses, we initially focused on targeted phosphopeptides. Hierarchical clustering of differentially abundant phosphosites confirmed the expected decrease in ERK1 Tyr204 and ERK2 Tyr187 phosphorylation with MEKi treatment, alongside an increase with growth factor treatment across all cell lines (Fig. 4A-C). Phosphorylation of EGFR Tyr1172 consistently increased across all cell lines in response to growth factor treatment, confirming established signaling patterns. Additionally, we observed a potentially synergistic increase in JNK1 phosphorylation at Tyr185 in both HCT116 and DLD1 cells, a site essential for JNK activation [41]. We note that the same phosphorylation site also maps to JNK3 (Tyr223), however this isoform is mostly expressed in the brain, heart and testes [42].

To more formally explore the synergistic regulation of targeted phosphorylation sites, we performed a factor analysis (Fig. S3A and Material and Methods). Briefly, we defined contrasts to evaluate the individual and combined effects of growth factors and MEKi, including a special "Interaction" contrast to detect synergies. A linear model with an empirical Bayesian estimate of variances and moderated t-test statistics was used to precisely assess the effects. This approach allowed us to accurately assess the influence of MEKi and growth factor stimulation on the levels of specific phosphopeptides, both separately and together. SPIED once again identified a larger number of regulated phosphosites, demonstrating its effectiveness (Fig. 4D). This analysis revealed synergistic regulation of a number of phosphorylation sites (Fig. S3B, S6). JNK was indeed synergistically activated in HCT116 and to a lesser extent in DLD-1 cells (Fig. 4E). In summary, our data indicates that MEK inhibition potentiates growth factor-induced JNK activation in HCT116 and DLD-1 cells. Also, the data underscores that focusing on a small number of functionally relevant phosphorylation sites yields clear, interpretable data.

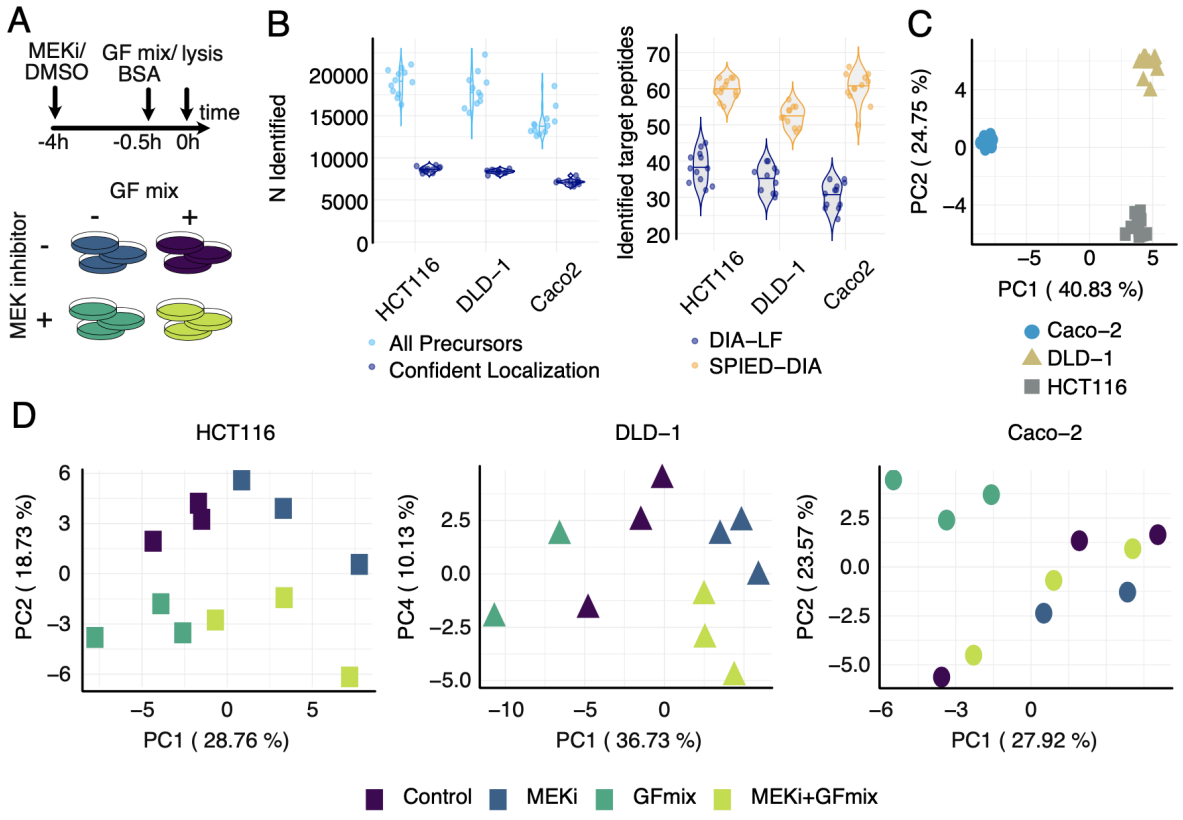

Figure 3. Overview analysis CRC cell-line panel treated with MEKi and growth factor mix. A. Experimental design of CRC panel treated with MEKi and growth factor mix (EGF, HGF, FGF2, and VEGF-C). B. Number of identified phosphopeptides per sample. Separated

according to all precursors and precursors with confidently localised phosphosites (left panel) and a comparison of identified target peptides between the label-free quantification pipeline and SPIED (right panel). C. Principal Component Analysis (PCA) of CRC cell lines, based on precursors identified in all samples in the label free results (n = 1699). D. PCA for HCT116, DLD-1, Caco-2 based on precursors identified in all runs per cell line in label-free analysis: 3423, 3476, and 3185 phosphopeptides, respectively. Each point represents a sample. Variance explained by principal components is indicated.

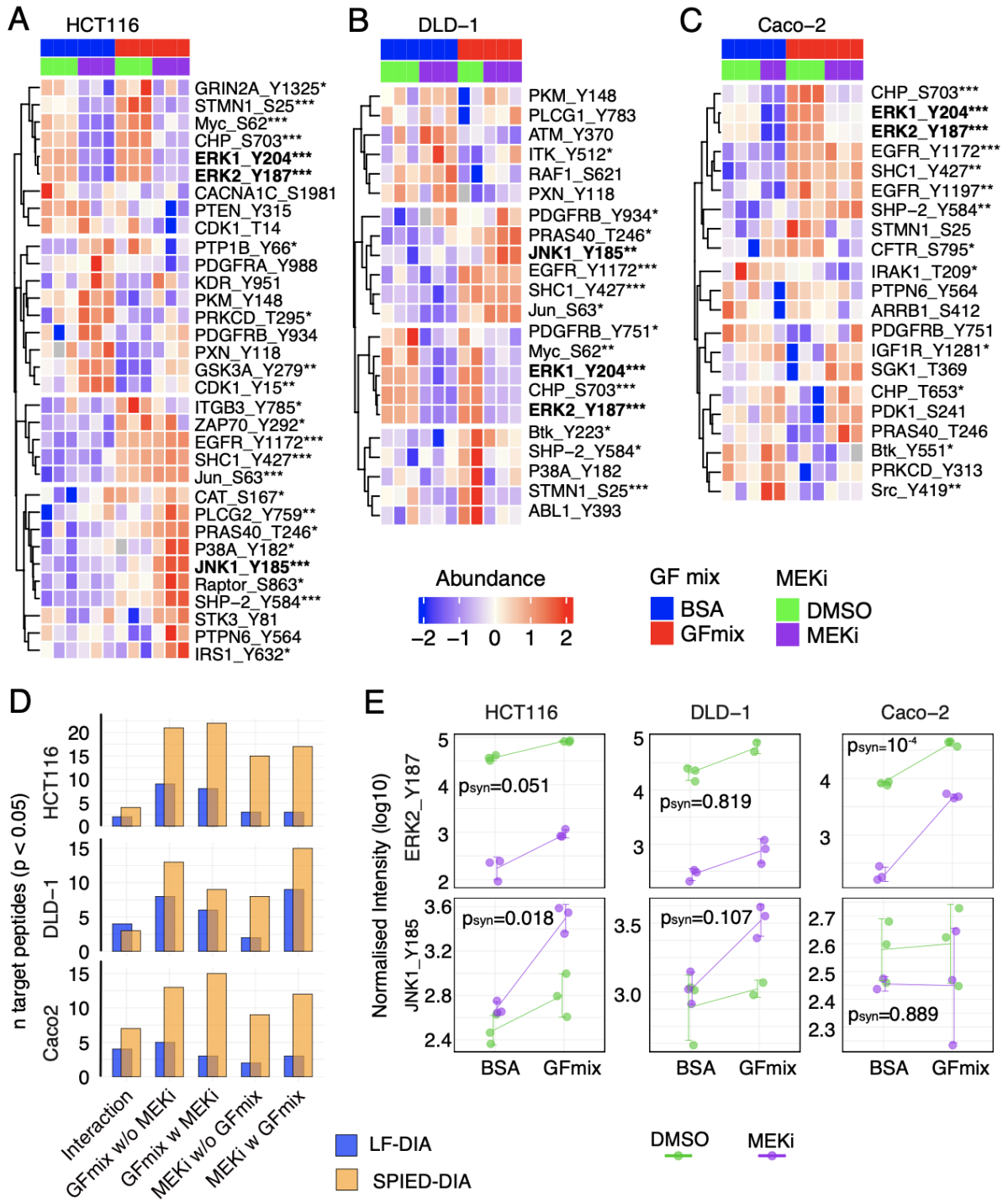

Figure 4: SPIED-DIA analysis of targeted regulated phosphorylation sites. Heatmaps display significant phosphosite regulation across different conditions in HCT116 (A), DLD-1 (B), and Caco-2 (C) cells. All depicted phosphosites passed an F-test p-value cut-off of 0.1. F-test P-values for specific sites is indicated by asterisks (*, $p < 0.05$; **, $p < 0.01$; ***, $p < 0.001$). Color scale represents row-wise Z-normalized abundance. D. Significantly regulated target phosphosites identified through label-free analysis. E. Log10 transformed loess-normalised precursor-level intensities of selected phosphorylation sites. Error bars indicate standard deviation and p-values derived from synergistic effect test with limma moderated t-test.

Global phosphoproteomics confirm synergistic activation of JNK signaling in HCT116 cells

A key advantage of SPIED-DIA is its ability to yield global phosphoproteomic data alongside the targeted analysis. We used these global data to complement the findings from our targeted study. Among the 22,326 phosphopeptide precursors passing our filtering criteria across all cell lines, 3,255 were identified as significantly regulated (Fig. S5B). Hierarchical clustering of these sites produced various clusters. Notably, cluster 6 in HCT116 cells and cluster 10 in DLD-1 cells exhibited patterns suggestive of synergistic signaling (Fig. S7, S8).

Kinase activity can be inferred from phosphoproteomic data using computational approaches [43–45]. To identify kinases involved in synergistic signaling in the global data, we performed enrichment analysis for cluster 6 and 10 in HCT116 and DLD-1 cells, respectively, using annotated kinase substrates from PhosphoSitePlus [14] and ikip-DB [46]. This analysis indicated synergistic activation of AKT1 in both HCT116 and DLD-1, consistent with the data from our screen (Fig. 3B). Although we included several AKT1 phosphorylation sites among our target peptides, the synthesis of heavy peptides failed, which explains their absence in the targeted data (Supplemental Table 1). Importantly, we also observed a significant enrichment of JNK1/2 targets in cluster 6 of HCT116 cells, supporting the results from the targeted analysis (Fig. 5A). This cluster contains the well known JNK target Jun Ser63 (Fig S7C). Hence, enrichment analysis of synergistic clusters identified kinase signatures consistent with the targeted data. Of note, no cluster indicating synergism was found in Caco-2 cells, consistent with the lack of synergistic signaling responses in this cell line (Fig. S9).

As an orthogonal way to analyze the global data, we also applied the factor analysis described above for each phosphorylation site identified in the global phosphoproteome. We then performed PTM signature enrichment analysis (PTM-SEA) [43] on phosphorylation site lists ranked by their fold-change signed p-values from the moderated t-test. Consistent with

the targeted analysis results, this revealed kinase activities aligned with established biological mechanisms. For example, the growth factor induced ERK1 and ERK2 signatures ("GFmix w MEKi" and "GFmix w/o MEKi") while MEKi reduced ERK1/2 signaling ("MEKi w GFmix" and "MEKi w/o GFmix"). We confirmed synergistic AKT activation in both HCT116 and DLD-1 cells, while JNK was only significantly activated in HCT116 (Fig. 5B, S10). In accordance with the SPIED-DIA data, no synergistic activation of JNK or AKT signaling was found in CaCo-2, based on the global data (Fig. 5B, S9, S10).

In summary, the targeted and global data highlighted the same pathways. We therefore proceeded with experimental validations, measuring cell growth in HCT116 and DLD-1 cells under specific targeted treatment combinations.

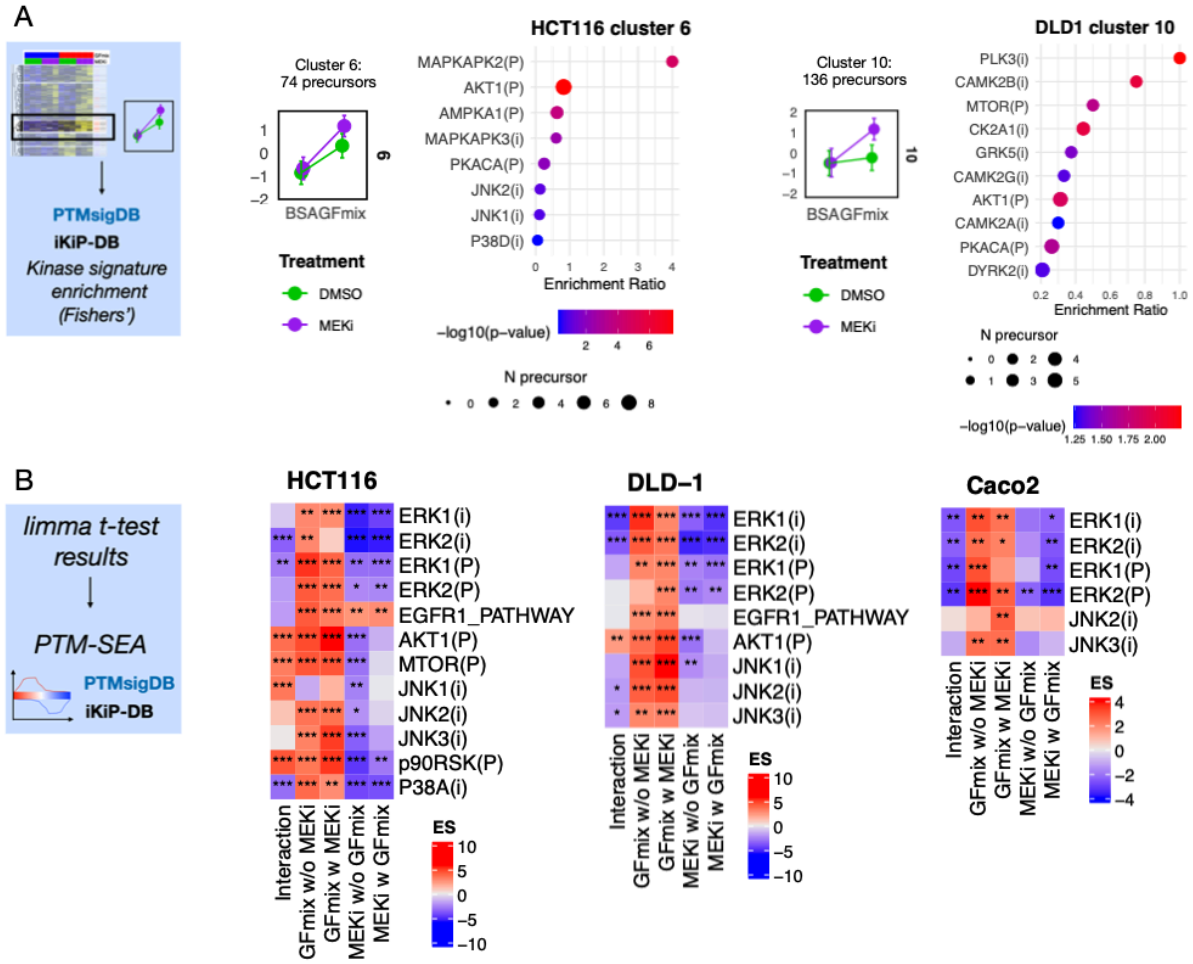

Figure 5: Analysis of label-free quantification data and kinase activity profiling. A. Kinase signature enrichment analysis of synergistic profile clusters from hierarchical clustered label-free data. Z-scored intensity profiles of treatment conditions within clusters. Data represented as mean ± standard deviation. Kinase signatures selected from PhosphoSitePlus and iKiP-DB. Size and color of points indicate number of precursors and significance (Fishers' exact test), respectively. B. Selected results from PTM-SEA using PhosphoSitePlus (PSP) and iKiP-DB kinase signatures, denoted by (P) and (i), respectively.

PTM-SEA input consists of fold change signed p-values from moderated t-test, filtered for phosphopeptides with F-test p-value < 0.1, indicating significant regulation in at least one test. ES = enrichment score as calculated by PTM-SEA. Significance is denoted by asterisks, with * p < 0.1, ** p < 0.05, *** p < 0.01.

JNK inhibition sensitizes CRC cells to MEKi

Our findings revealed the involvement of both JNK and PI3K/AKT/MTOR pathways in the synergistic signaling responses to MEK inhibition. This indicates that combining MEKi treatment with drugs targeting JNK or PI3K/AKT/MTOR could be a promising strategy for combinatorial therapy. To assess this experimentally, we treated HCT116 and DLD-1 cells with MEKi and either a JNK inhibitor (JNK-in-VIII) or a PI3K inhibitor (GDC-0941) in different concentrations and monitored cell growth over 48 hours via live cell imaging (Fig. 6A).

We observed a synergistic effect of MEKi and PI3Ki on DLD-1 and HCT116 growth (Fig 6B, C), confirming previous reports of KRAS mutated CRC models, including HCT116 and DLD-1 cells [6,47–52]. The JNK inhibitor (JNKi) had minimal effect on DLD-1 cell division, both alone and when combined with MEKi (Fig. 6D and 6E). In contrast, a 5 μM dose of JNKi significantly slowed the division of HCT116 cells, nearly doubling the cell division time. MEKi alone exhibited a more modest impact, even at the highest concentration tested. Notably, while low doses of JNKi or MEKi alone did not significantly affect HCT116 cell division, their combination markedly inhibited cell growth (Fig. 6D). Specifically, 1 μM JNKi or 0.2 μM MEKi alone extended HCT116 cell cycle times from 25 to 27 hours, but combining both drugs increased this to 37 hours. Hence, MEK inhibition sensitizes HCT116 cells to JNKi. Collectively, these results show that our targeted phosphoproteomic approach has uncovered synergistic signaling responses that are functionally relevant.

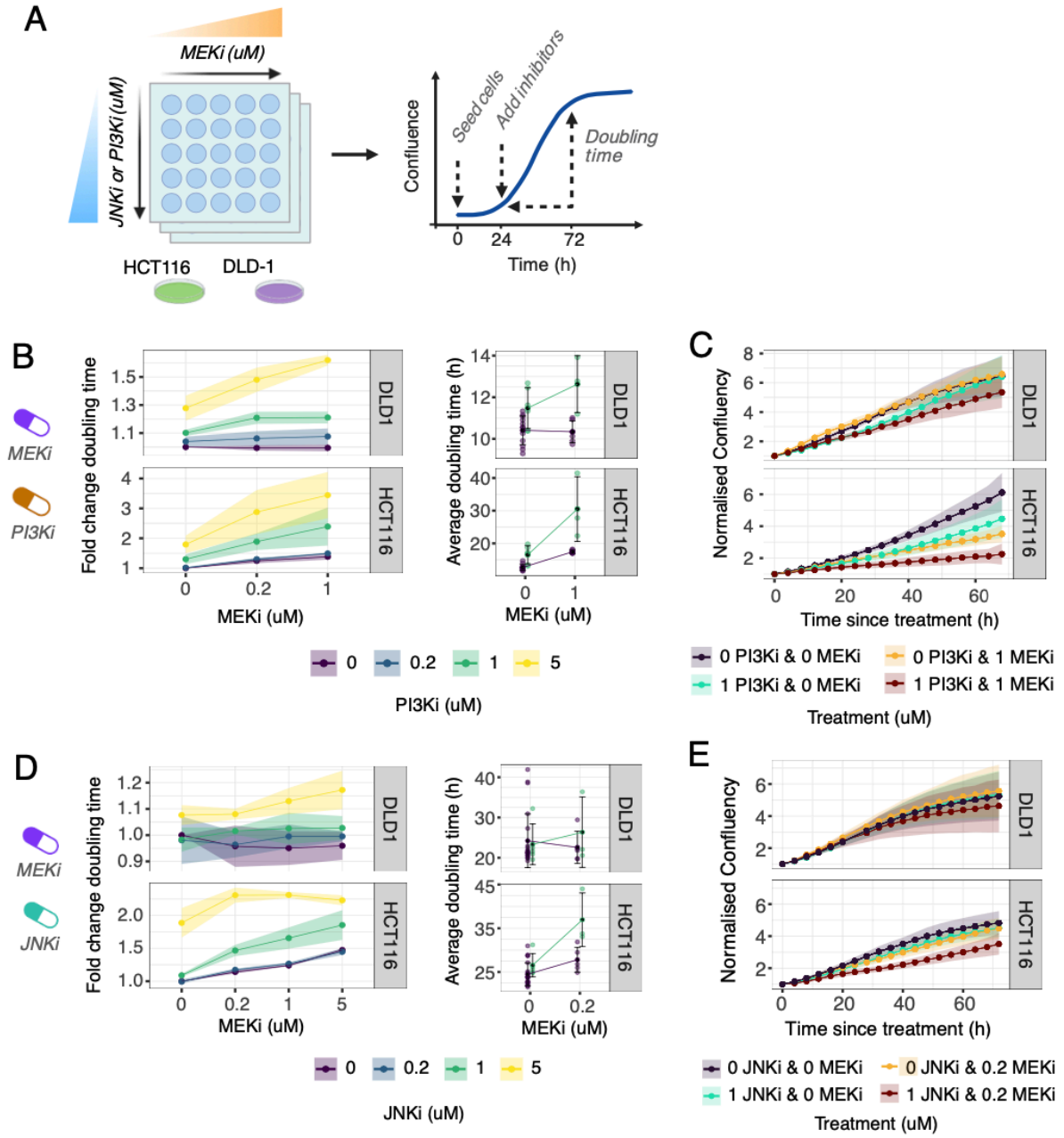

Figure 6: Experimental workflow and results for combination treatment with MEKi and JNKi or PI3Ki. A. Experimental workflow depicting inhibitor treatment of cell lines prior to measurement of cell growth and doubling time with live-cell imaging. B. Cell doubling time fold changes relative to within replicate controls, 48 hours post-treatment with inhibitors. Insets depict doubling times at selected concentrations. C. Growth curves of cells within selected treatment conditions, normalized to treatment-start. D/E. Similar to panels B and C, these graphs display the effects of combining MEKi with JNKi on cell doubling time and growth curves. Data are presented as mean ± standard deviation, shaded ribbons also indicate standard deviation.

Discussion

In this study, we explored synergistic signaling in colorectal cancer cell lines by integrating DIA with spike-in synthetic heavy stable isotope-labeled phosphopeptides, enhancing the detection of specific phosphopeptides. Our method, SPIED-DIA, marries the sensitivity of targeted detection with DIA's broad discovery capabilities, offering a streamlined approach that doesn't require specialized data acquisition schemes and is compatible with standard mass spectrometers, simplifying the detection of key phosphorylation sites while leveraging the full benefits of label-free DIA phosphoproteomics. Despite these advantages, SPIED-DIA also has limitations. SPIED-DIA provides only a modest sensitivity boost for target peptides because it lacks the longer selective ion collection periods found in other targeted approaches [27,28,35]. Moreover, like other spike-in strategies, obtaining target-specific heavy reference peptides is challenging and expensive. To economize, we opted for pooled synthesis of heavy reference peptides. However, this approach led to unsuccessful synthesis of some desired peptides, rendering them unusable in our targeted strategy. A viable alternative is utilizing off-the-shelf reference peptide collections like the PQ500 standard for plasma proteomics (Biognosys) or the recently introduced multipathway phosphopeptide standard[53]. Another advantage of these standardized sets is that they also enhance data consistency across different research labs. The community would benefit if other target sets like the SigPath and T-loop libraries were to also become commercially available [24,25].

In CRC, the classical MAPK signaling pathway is chronically activated, often by mutations in RAS or RAF [54]. This suggests that inhibiting the central kinase, MEK, could be a valid therapeutic strategy. However, signaling in CRCs rewires due to strong feedbacks leading to cross-activation of parallel pathways [7,55], often mediated by the EGF receptor. Based on a screen with 11 CRC cell lines and different growth factors, we observed that MEKi-induced synergistic AKT activation is not only mediated by EGF but also by HGF, FGF2 and VEGF-C. We then applied SPIED-DIA to investigate synergistic signaling responses in three selected cell lines in detail. Our results highlight the key advantages of the SPIED-DIA approach. Firstly, the targeted analysis of functionally relevant phosphorylation sites provides easily interpretable data that directly highlight key changes in cell signaling. Secondly, the global data obtained in parallel can be used to extract kinase activity profiles. Interestingly, both approaches revealed synergistic activation of JNK signaling in HCT116 cells, suggesting that combinatorial treatment with MEKi and JNKi could be an attractive therapeutic option. The consistency between the datasets not only validates

our analytical strategy but also solidifies our confidence in these candidate pathways as critical mediators of the cellular response in our study model. Indeed, we confirmed that JNK inhibition sensitizes HCT116 cells to MEKi treatment, leading to marked reduction in cell proliferation. In addition to EGF, JNK was also activated by HGF and FGF2, supporting the notion that synergistic signaling can also be mediated by other receptors than EGFR.

Oncogenic signaling in CRC involves multiple pathways, notably EGFR/MAPK, WNT, Pi3K/Akt, JAK/STAT, Notch, SHH, and TGF-beta [3,56]. Given that JNK is not typically linked to oncogenic signaling in CRC, our observation of its synergistic activation upon MEK inhibition is initially surprising. However, our data does align with known MEK-JNK interactions. MEK activation typically upregulates DUSP4, which inactivates JNK [57,58]. Additionally, cancer cells with loss of function mutations in MAP3K1 or MAP2K4, which activate JNK, are often sensitive to MEK inhibitors, highlighting the functional relevance of the ERK-JNK crosstalk [59]. Very recently, the $KRAS^{G12C}$ inhibitor sotorasib and the MAP2K4 inhibitor HRX-0233 were shown to synergistically inhibit growth of a number KRAS mutant CRC and lung cancer cell lines and to induce durable tumor shrinkage in mouse xenografts of human lung cancer cells [60]. Although this recent study focused on different kinases, its findings bolster the concept of synergistically targeting MEK/ERK and JNK signaling as a viable approach in cancer therapy.

Selecting optimal treatments to target cancer remains an important challenge. In this study, we demonstrate that targeted phosphoproteomics using SPIED-DIA can reveal signaling responses, which can help predict effective combinatorial treatments. While the work presented here is limited to cancer cell lines, the technology also has the potential to be applied to patient samples. For example, microscaled phosphoproteomic techniques have successfully identified 7,000 phosphosites in retrospective formalin-fixed paraffin-embedded (FFPE) tissue samples [61]. In addition, combining ultrasensitive proteomics with laser tissue microdissection facilitates spatial proteomics in human tissues [62,63]. In the future, integrating these technologies with SPIED-DIA promises to reveal signaling pathways and predict treatments directly in patient samples.

Materials and Methods

Cell culture and treatment experiment

HCT116, Caco2 and DLD1 were obtained from ATCC (Manassas, Virginia, USA). Cell lines were confirmed to be mycoplasma free. All cell-lines were cultured in DMEM, high glucose, GlutaMAX Supplement, pyruvate (Gibco, Invitrogen), supplemented with 10% fetal bovine serum (FBS, Gibco), in a humidified incubator at 37 °C with 5% CO^2. Experiments are performed at 80% confluence. Cells are harvested in ice cold PBS, by washing two times in ice cold PBS, and scraping from plate. The cells were rinsed again with 1× PBS and centrifuged at 250g for 5 min in a centrifuge maintained at 1 °C. The final PBS wash was removed and the resulting pellet was frozen in ethanol on dry ice and stored at −80 °C.

Treatment with Growth Factor and MEK Inhibitor

For the interaction experiment, we used the MEK inhibitor Selumetinib (AZD6244, #S1008, Selleckchem) at a final concentration of 10 µM, dissolved in DMSO. The growth factors used were HGF (Peprotech #100-39H, final concentration 0.025 µg/ml), FGF2 (Peprotech #100-18B, final concentration 0.005 µg/ml), EGF (Peprotech #AF-100-15, final concentration 0.025 µg/ml), and VEGF-C (Peprotech #100-20CD, final concentration 0.1 µg/ml), all of which were dissolved in 0.1% BSA. Depending on the specific experiment, these growth factors were either added individually or combined into a mixture.
Prior to treatment, the cells underwent a starvation period of approximately 18 hours using 0.1% FBS to synchronize their growth. Following this, the cells were treated with either MEKi or a control solution of DMSO for 3.5 hours. At 3.5 hours either a control solution (0.1% BSA) or the growth factor (mixture) was added to the cells for another 30 minutes. After a total incubation time of 4 hours, the cells were harvested for further analysis.

Selection and synthesis spike-in peptides

Phosphosites were selected for relevance to cellular signaling. The Kinase-Substrate, Phosphorylation-site and Regulatory-site datasets were downloaded from PhosphoSitePlus (February 2018). Phosphorylation sites that are present in all three datasets, annotated to regulate protein activity and annotated to selected KEGG signaling pathways. Phosphosites annotated to manually selected proteins (CREB1, ABL1, IGF1R, IRS1, RPS6KA1, PDGFRA, PIK3R1 and RPS6) or with more than 100 references were kept in regardless of activity and pathway annotation. This results in a list of ~1000 phosphorylation sites. These phosphorylation sites were mapped to an in-silico trypsin digested proteome, and the resulting phosphopeptides were filtered based on their MS properties. The peptide is not allowed to be found in the proteome >10 times and it can not contain >10 phospho-accepting residues. Phosphopeptides were filtered for synthesis feasibility, and singly phosphorylated peptides with a length between 7 and 21 amino acids and N-terminal K/R were selected for synthesis. The list with shorter peptides contains 524 phosphorylation sites, mapping to 485 unique phosphopeptides, on 277 proteins. Peptides were purchased from JPT, synthesized using FMOC solid-phase technology with crude purity and synthetic isotope–labeled c-terminal lysine (K) or arginine (R) and pooled. Lyophilized synthetic peptides were kept at -20.

Phosphoproteomics sample preparation

Cell pellets were lysed at 4 °C with urea lysis buffer (8 M urea, 50 mM Tris (pH 8),150 mM

NaCl) supplemented with protease inhibitors (2 µg/ml aprotinin, 10 µg/ml leupeptin) and phosphatase inhibitors (10 mM NaF, phosphatase inihibitor cocktail 1 and 2, Sigma Aldrich). The cell lysate was treated with 5 mM dithiothreitol for 1 h to reduce proteins and then alkylated with 10 mM iodoacetamide for 45 min in the dark. Sequencing grade LysC (Wako) was added at a weight to weight ratio of 1:50. After 2 h, samples were diluted 1:4 with 50 mM Tris–HCl pH 8 and sequencing grade trypsin (Promega) was added at 1:50 ratio. Digestion was completed overnight. subsequently samples were acidified using FA and desalted with Sep-Pak C18 cc Cartridges (Waters). Lyophilized samples are diluted to 0.7 µg/µL in 80% ACN / 0.1% TFA. 200 fm heavy labeled synthetic peptides are added to 100ug sample and subjected to automated immobilized metal affinity chromatography (IMAC) phosphopeptide enrichment by the Bravo Automated Liquid Handling Platform (Agilent) with AssayMAP Fe(III)-NTA cartridges.[64]

Liquid chromatography mass spectrometry

Mass spectrometry raw data were acquired on a Bruker timsTOF Pro2 connected to a Thermo Fischer EASY-nLC 1200 system. Around 300 ng (⅓ of IMAC output) was injected. Samples were separated online on a 25 cm column packed in-house with C18-AQ 1.9 µm beads (Dr. Maisch Reprosil-Pur 120). A gradient of mobile phase A (0.1% formic acid and 3% acetonitrile in water) and mobile phase B (0.1% formic acid, 90% acetonitrile in water) was used to separate the peptides at a flow rate of 250 nl/min. Mobile phase B was ramped from 2% to 30% in the first 29 min, followed by an increase to 60% B in 3 min and a plateau of 90% B for 5 min. Temperature of the column was kept constant at 45 °C. The LC system was connected to Bruker timsTOF Pro2 hybrid TIMSQTOF mass spectrometer via a CaptiveSpray nano-electrospray source. The raw files were acquired in dia-PASEF mode, using the standard 'long gradient' method as supplied by the vendor. All spectra within a mass range of 400 to 1201 Da and an IM range from 1.6 to 0.6 V·s/cm^2 were acquired using equal ion accumulation and ramp times in the dual TIMS analyzer of 100 ms each. The collision energy was lowered as a function of increasing ion mobility from 59 eV at 1/K0 = 1.6 V·s/cm^2 to 20 eV at 1/K0 = 0.6 V·s/cm^2. The estimated cycle time is 1.80s. The calibration status of the machine is monitored constantly and calibration of the ion mobility dimension is performed linearly using at least three ions from Agilent ESI LC/MS tuning mix (m/z, 1/K0: 622.0289, 0.9848 V·s/cm^2; 922.0097, 1.1895 V·s/cm^2; 1221.9906, 1.3820 V·s/cm^2).

Benchmark sample generation and High-pH Reverse-Phase Fractionation for Library Generation

For the High pH library generation HCT116 was treated with combinations of phosphatase inhibitors, to increase the number detectable phospho-site relative to normal growth conditions. For inhibition of phosphatases, HCT116 (ATCC, #7) was treated with 1 mM pervanadate and 50 ng/ml calyculin A. To this end, cells were starved in 0.1% FBS for 3 hours. afterwards cells were treated with no serum, with 10% FBS, 10% FBS + calyculin A, or 10% FBS + calyculin A + Pervanadate. Samples were processed as described before, and desalted peptides were combined before drying down.

For library generation, the peptides are subjected to offline high pH reverse phase fractionation by HPLC on an Agilent 1290 Infinity II HPLC instrument. To this end, the dried peptides were reconstituted in high pH buffer A (4.5 mM ammonium formate, 2% ACN, pH 10), and loaded on a XBridge BEH C18 4.6 × 250 mm column (130Å, 3.5 µm bead size; Waters), and separated using a 96-min gradient with a flow rate of 1 ml/min. The gradient was performed by ramping high pH buffer B (4.5 mM ammonium formate, 90% ACN, pH 10)

from 0% to 60% [64]. The 96 fractions were collected and concatenated by pooling equal interval fractions. The final 48 fractions were dried down and resuspended for IMAC enrichment as described above. 100 µg of each pooled fraction were used for IMAC enrichment. Per IMAC enriched fraction 100 ng phospho-enriched peptides were measured on the timsTOF Pro2.
Same LC conditions as described previously were used. Data were acquired using default DDA-PASEF mode with a cycle time 1.1s and 10 PASEF MS/MS scans per topN acquisition cycle. All spectra were acquired within an m/z range from 100 to 1700 and an IM range from 1.6 to 0.6 V·s/cm^2
Raw data was analyzed with MaxQuant (v2.4.0.0) and searched against the human reference proteome database (downloaded from UniProt in 06/2023) and default protein contaminants included in MaxQuant. Fixed modifications were set to carbamidomethylation of C. Variable modifications included oxidation (M) and N-terminal acetylation and phosphorylation (STY). A maximum of 5 modifications per peptide and 2 missed cleavages were allowed. MaxQuant results are filtered to exclude reverse database hits, potential contaminants and phospho-sites with a localisation probability lower than 50%. MaxQuant results were transformed and were necessary combined to a DIAN-NN compatible library, including ion mobility information.

Synthetic peptides library generation
The synthetic phosphopeptides were measured to generate a library. The peptides were dissolved in Buffer A (3% ACN, 0.1% FA). To generate a library, 50 fm and 100 fm peptides were measured in DDA-PASEF mode in triplicates, with the same settings as for HpH-library generation acquisition. The resulting raw files were analysed in MaxQuant against a library specific .fasta file. MaxQuant settings and processing of MaxQuant output as above. A table with peptides in the library, along with main annotated phosphosite and other annotated phosphosites can be found in supplementary table 1.

Full phospho-proteome dilution benchmark
For dilution series with the SILAC labeled phosphoproteome HCT116 was cultured in Heavy or Light SILAC medium. SILAC medium consists out of arginine- and lysine- free DMEM, supplemented with 10% dialyzed fetal bovine serum (dFBS, Gibco) and either heavy (13C615N4 L-arginine or Arg10 an 13C615N2 L-lysine or Lys8) and light amino acids (Cambridge Isotope Laboratories) at 0.4 mmol/L and 0.8 mmol/L. Cell harvest and lysis as described above. Protein concentration in cell lysate was determined using BCA and the heavy labeled cell lysate was sequentially diluted into the light cell lysate. Subsequent sample preparation and phosphopeptide enrichment were performed as usual. For mass spectrometry 100 ng phospho-enriched peptides per sample were injected per dilution in triplicates and analysed in DIA-PASEF mode, as described above.

Cell line panel screen for MEKi-dependent receptor-mediated feedbacks
Bio-Plex data generation
Human colorectal cell-lines used in this experiment Colo205, Colo678, DLD-1, GEO, HCT116, HT29, LIM1215, RKO, SW403, SW480 and Caco-2 were provided by AG Sers Molekulare Tumorpathologie (Charité-Universitätsmedizin). All cell-lines were cultured in low glucose DMEM (D5546-6X500ML, Sigma-Aldrich) supplemented with 10% FBS, 10mM Ultraglutamine and Penicilin-Streptomycin and were incubated at 37°C and 5% CO_2.
Before perturbation commenced cells were starved overnight in serum free medium. At 4h

before lysis the cells were treated with 1µM AZD6244 (Selleckchem, S1008) or solvent control DMSO and at 20 minutes before lysis cells were stimulated with ligands, full serum (10% FBS) or solvent control PBS/BSA (n=4 replicates). We used the following ligands (all Peprotech): EGF (25ng/ml), HGF (50ng/ml), IGF1 (100ng/ml), FGF2 (5ng/ml), PDGF (10ng/ml), VEGF-B (100ng/ml) and VEGF-C (100ng/ml). After treatment and incubation, lysates were collected and analyzed with the Bio-Plex Protein Array system (Bio-Rad, Hercules, CA) as described earlier using magnetic beads specific for AKT^{S473}, $ERK1/2^{T202,Y204/T185,Y187}$ and $MEK1^{S217,S221}$. The beads and detection antibodies were diluted 1:3. For data acquisition, the Bio-Plex Manager software and the R package lxb was used.

Bio-Plex data processing

First, obvious outliers among replicates exhibiting an absolute z-score >=3 for all three phosphosite measurements were removed. For each cell-line, data were processed separately for each of the 3 measured phosphoproteins. The value of the control (PBS/BSA+DMSO) was estimated as the mean value of the replicates and log2 fold changes with respect to the control were then computed for all conditions. The resulting fold changes x where then used to calculate the hyperactivation effect of GF and AZD on pAKT:

$AKT_{interaction\_FC} = \mu(x_{GF+AZD}) - \mu(x_{GF+DMSO}) - \mu(x_{BSA+AZD}) - \mu(x_{BSA+DMSO})$.

To estimate the significance of this hyperactivation we conducted a two-way anova analysis with interaction term and ascribed synergistic hyperactivation if meeting the following three criteria: (i) significance ($p<=0.05$), (ii) synergy ($AKT_{interaction\_FC}>0$) and (iii) receptor dependency ($AKT_{interaction\_FC}(GF) > AKT_{interaction\_FC}(PBS/BSA)$ in the same cell line).

SPIED-DIA analysis

Raw file processing

For the label-free analysis of the raw files, the raw files were processed using DIA-NN (v1.8.2 beta 11), with searches conducted against the library derived from the target peptides only (generated as described above) and reannotation enabled. Settings included methionine excision and *in silico* digestion at K/R, with cysteine carbamidomethylation as a fixed modification. Variable modifications included methionine oxidation, N-terminal acetylation, and phosphorylation on STY, with phosphorylation scored independently. The analysis allowed for one missed cleavage and a maximum of three variable modifications. The “report-lib-info” option was activated to facilitate raw data verification in subsequent stages. SILAC labeling with a mass delta of 0 at KR was applied as a fixed modification, SILAC channels L (K[0], R[0]), H (K[8.0142], R[10.0083]), and a decoy (K[16.0284], R[20.0165]) were registered.

Process DIA-NN output

Data are filtered to only include Heavy channel entries (spike-in), Channel.Q.Value < 0.05, PTM.Q.Value < 0.05, PTM.Site.Confidence > 0.5 and a Channel.H > 1000 (spike-in intensity). Furthermore, precursors need to have Channel.L (light, endogenous intensity) > 900 in at least 1 condition to ensure no noise-to-noise comparisons and the light precursor needs to be identified with a Channel.Q.Value < 0.5 in at least 3/12 samples. Subsequently, for the precursors passing the filters, a “rescalingfactor” is calculated using the median of Channel H intensities, and light intensities are rescaled to log10-transformed ratios of Channel L to Channel H, adjusted by this factor like such: log10((Channel.L/Channel.H)*rescalingfactor. This transformation is applied to mitigate intensity disparities and inspired by the RefQuant approach[30]

The rescaled intensities are normalized using the normaliseCyclicLoess function from the limma package. The differential abundance analysis is performed as described in the

label-free data analysis pipeline. Precursors are grouped by unique phosphopeptide sequence and filtered for precursors with the lowest F-test p value. Precursors with an F test p value < 0.1 or 0.2 (indicated below relevant figures) are selected for visualization in a heatmap.

Visualization raw data

For the visualization of the raw MS/MS spectra, which facilitates validation of phosphorylation site localisation and the identification of stable isotope-labeled fragments, we employed the following procedure: the ScanID was retrieved from the DIA-NN output table. To determine the corresponding exact scan number from the Bruker raw file, we treated the approximate scan number as the absolute number of MS/MS scans within the run. The exact scan number was then directly derived from the raw data file itself. Subsequently, the MS/MS spectra were downloaded using the Bruker Data Analysis tool. Relevant peaks within the spectra were manually annotated in R using the spectral library as used for the DIA-NN analysis within a 10 ppm mass accuracy range and plotted.

Label-free DIA analysis

Raw file processing

For the label-free analysis of the raw files, the raw files were processed using DIA-NN (v1.8.2 beta 11), with searches conducted against the high pH library (generated as described above) and reannotation enabled. Settings included methionine excision and *in silico* digestion at K/R, with cysteine carbamidomethylation as a fixed modification. Variable modifications included methionine oxidation, N-terminal acetylation, and phosphorylation on STY, with phosphorylation scored independently. The analysis allowed for one missed cleavage and a maximum of three variable modifications. The “report-lib-info” option was activated to facilitate raw data verification in subsequent stages.

Filter and normalise DIA-NN output

DIA-NN output was processed in R (v4.3.0) filtered with Q.Value < 0.05, only phosphorylated precursors, PTM.Site.Confidence > 0.5 and PTM.Q.Value < 0.05 (Fig. S1B). Precursor intensities (Ms1.Area) were log10-transformed and collectively normalised to correct for loading bias between samples using loess (function: normalizeCyclicLoess) from the limma package (v3.56.1)[65]. No imputation was performed at any stage in the analysis. PCA was performed on precursors identified in every sample within a group (all cell lines together or individual cell lines).

Differential abundance analysis

Differential abundance analysis of phosphopeptides within cell lines, across conditions, was conducted using the limma package, employing a factorial analysis approach with MEKi and GFmix as factors in the linear model. Precursors were filtered to include only those with a maximum of five missing values. Within the factorial design, contrasts were strategically defined to investigate synergistic effects: the differential impact of the growth factor mix with and without MEKi ("GFmix w MEKi" and "GFmix w/o MEKi"), and conversely, the effect of MEKi with and without the growth factor mix ("MEKi w GFmix" and "MEKi w/o GFmix"). Potential synergistic interactions were explored through an "Interaction" contrast. A linear model was fitted to the data and Bayesian statistics (*ebayes* function limma) were then applied to estimate variance among the precursors, employing moderated t-statistics and moderated F-statistics. Results were extracted and aggregated for further analysis. Especially, precursors are grouped per unique phosphopeptide sequence and the precursor with lowest p-value from the moderated F-test is selected for downstream analysis.

Clustering significantly interesting phosphosites and investigation interesting clusters

Precursors with F p-values < 0.05 or 0.1 (as indicated below figure), indicating significant regulation, were selected and displayed in a heatmap. Hierarchical clustering was used to organize the heatmap, with the number of clusters determined manually to best represent the data. For each cluster, means of z-score normalized precursors were calculated. Clusters suggesting synergistic interactions between GFmix and MEKi were specifically identified for further analysis. Kinase signatures from PTMsigDB and iKIP-DB were used to perform kinase overrepresentation analysis via Fisher's exact test, identifying enriched kinase activities linked to the treatment effects.

PTM-SEA analysis

PTM signature enrichment analysis (PTM-SEA, https://github.com/broadinstitute/ssGSEA2.0) was employed to infer kinase activity from regulated phospho-sites. Precursors with a p-value lower than 0.1 as derived from the limma moderated F-statistics (regulated phosphopeptides) were selected. As input we used signed (according to log2 fold change) -log10-transformed p-values per comparison, derived from moderated t-test. PTM signatures were sourced from PTMsigDB[43] (v2.0.0) and iKIP-db[46]. As unique site identifiers, the 14 amino acid phospho-site flanking sequence window was used. Multiply phosphorylated peptides were split per phosphorylation site. PTM-SEA was run with sample.norm.type set to "none" and weight to "1".

Growth curves inhibitor combination treatment HCT116 and DLD1

Combination Treatment

The effects of combination treatment were assessed by monitoring cell proliferation and death through live-cell imaging. In validation experiments, HCT116 and DLD1 cell lines were treated with combinations of a MEK inhibitor (AZD6244) and either a JNK inhibitor (JNK-IN-8, S4901, Selleckchem) or a PI3K inhibitor (Pictilisib, GDC-0941, S1065, Selleckchem). Cells were seeded at densities of 4000 cells per well for HCT116 and 2500 cells per well for DLD-1 in 96-well plates and cultured in the described growth medium. Twenty-four hours post-seeding, cells were treated with inhibitor combinations at concentrations of 0 (duplicated for double-negative controls), 0.2, 1, and 5 µM, using a quadratic mixing format. To mitigate edge effects, outer rows were left empty and filled with PBS. Cell growth was monitored for an additional three days post-treatment. Experiments were performed in biological triplicates. For treatments combining MEK and JNK inhibitors, the protocol included an additional condition where the medium was supplemented with growth factors (HGF, EGF, and FGF) at specified concentrations.

Incucyte Live Cell Imaging

Automated phase-contrast and green-fluorescent long-term imaging was conducted using an Incucyte instrument (dual-color model 4459, Incucyte Essen Bioscience) in a standard humidified incubator at 37°C and 5% CO2. Imaging occurred every four hours, capturing four frames per well using a Nikon 10x objective.

Image Processing

Images were processed using Incucyte ZOOM software (2018A) with the manufacturer's default masking settings. Confluence values (percentage of area covered by the confluence mask) were exported for further analysis. Image frame data were individually exported and processed in R.

Growth was assessed in multiple ways: raw growth curves were examined for outliers and excluded from further analysis. To determine changes in doubling time, the doubling time in the 48 hours post-treatment was compared to the baseline (0 µM concentration) within each

replicate. The average doubling time for selected concentrations of interest was summarized across all replicates. The growth curves for selected concentrations were normalized to the confluence at time zero (treatment) within each well or image frame.

Data availability

Mass spectrometry raw files as well as MaxQuant and DIA-NN output tables, spectral libraries and processed data have been deposited to the ProteomeXchange Consortium via the PRIDE [66] partner repository. The accession ID is PXD050961.

Contributions

M.V.B., B.K., N.B. and M.S. contributed to the design and conceptualisation of this study. The phosphosites in the panel were selected by N.B., B.K. and M.V.B.. Experimental work was performed by M.V.B., A.S., N.L., M.H., S.Na and S.Ni.. Analysis of experimental data was conducted by M.V.B., supervised by N.B., M.S. and B.K.. The data was mostly visualised by M.V.B. and partly by B.K.. The manuscript was written by M.S., M.V.B. and N.B. with editing and contributions from all co-authors.

Acknowledgements

We would like to thank Martha Hergeselle (MDC) for her assistance with cell culture and Christian Sommer (MDC) for technical support. We also thank Henrik Zauber, Anna Welter, and Robert Kerridge (all MDC) for their valuable discussions on quantification strategies. Additionally, we express our gratitude to Vadim Demichev (Charité) for his advice on data analysis using DIA-NN. This work was supported by the German Ministry of Education and Research (BMBF) through the national research node for mass spectrometry in systems medicine, MSTARS (16LW0240 and 16LW0239K), awarded to M.S. and N.B., and the German Research Foundation (CRC1588), awarded to N.B. and M.S. Additional funding for M.V.B. was provided by the Deutsches Konsortium für Translationale Krebsforschung (DKTK) and the Berlin School for Integrative Oncology (BSIO). B.K. was supported by Deutsche Krebshilfe (DKH, 70114307).

References

1. Hanahan, D. Hallmarks of Cancer: New Dimensions. *Cancer Discov.* **12**, 31–46 (2022).
2. Cohen, P., Cross, D. & Jänne, P. A. Kinase drug discovery 20 years after imatinib: progress and future directions. *Nat. Rev. Drug Discov.* **20**, 551–569 (2021).
3. Xie, Y.-H., Chen, Y.-X. & Fang, J.-Y. Comprehensive review of targeted therapy for colorectal cancer. *Signal Transduct. Target. Ther.* **5**, 22 (2020).
4. Britschgi, A. *et al.* JAK2/STAT5 Inhibition Circumvents Resistance to PI3K/mTOR Blockade: A Rationale for Cotargeting These Pathways in Metastatic Breast Cancer. *Cancer Cell* **22**, 796–811 (2012).
5. Dorel, M. et al. Neuroblastoma signalling models unveil combination therapies targeting feedback-mediated resistance. *PLoS Comput. Biol.* **17**, e1009515 (2021).
6. Klinger, B. et al. Network quantification of EGFR signaling unveils potential for targeted combination therapy. *Mol. Syst. Biol.* **9**, 673–673 (2013).
7. Prahallad, A. et al. Unresponsiveness of colon cancer to BRAF(V600E) inhibition through feedback activation of EGFR. *Nature* **483**, 100–103 (2012).
8. Frejno, M. et al. Proteome activity landscapes of tumor cell lines determine drug responses. *Nat Commun* **11**, 3639 (2020).
9. Grossbach, J. et al. The impact of genomic variation on protein phosphorylation states and regulatory networks. Mol. Syst. Biol. **18**, e10712 (2022).
10. Gerritsen, J. S. & White, F. M. Phosphoproteomics: a valuable tool for uncovering molecular signaling in cancer cells. *Expert Rev. Proteom.* **18**, 661–674 (2021).
11. Aebersold, R. & Mann, M. Mass-spectrometric exploration of proteome structure and function. Nature **537**, 347–355 (2016).
12. Riley, N. M. & Coon, J. J. Phosphoproteomics in the Age of Rapid and Deep Proteome Profiling. *Anal Chem* **88**, 74–94 (2016).
13. Olsen, J. V. et al. Global, in vivo, and site-specific phosphorylation dynamics in signaling networks. Cell **127**, 635–48 (2006).
14. Hornbeck, P. V. et al. PhosphoSitePlus, 2014: mutations, PTMs and recalibrations. *Nucleic Acids Res.* **43**, D512–D520 (2015).
15. Mertins, P. et al. Proteogenomics connects somatic mutations to signalling in breast cancer. Nature **534**, 55–62 (2016).
16. Demichev, V., Messner, C. B., Vernardis, S. I., Lilley, K. S. & Ralser, M. DIA-NN: neural networks and interference correction enable deep proteome coverage in high throughput. *Nat. Methods* **17**, 41–44 (2020).
17. Demichev, V. et al. dia-PASEF data analysis using FragPipe and DIA-NN for deep proteomics of low sample amounts. *Nat. Commun.* **13**, 3944 (2022).
18. Meier, F. et al. diaPASEF: parallel accumulation–serial fragmentation combined with data-independent acquisition. Nat. Methods 17, **12**29–1236 (2020).
19. Bekker-Jensen, D. B. et al. Rapid and site-specific deep phosphoproteome profiling by data-independent acquisition without the need for spectral libraries. Nat Commun 11, 787 (2020).
20. Oliinyk, D. & Meier, F. Ion mobility-resolved phosphoproteomics with dia-PASEF and short gradients. *PROTEOMICS* **23**, e2200032 (2023).
21. Skowronek, P. et al. Rapid and In-Depth Coverage of the (Phospho-)Proteome With Deep Libraries and Optimal Window Design for dia-PASEF. *Mol. Cell. Proteom.* **21**, 100279 (20**22**).

22. Kitata, R. B. et al. A data-independent acquisition-based global phosphoproteomics system enables deep profiling. Nat. Commun. 12, 2539 (2021).
23. Srinivasan, A., Sing, J. C., Gingras, A.-C. & Röst, H. L. Improving Phosphoproteomics Profiling Using Data-Independent Mass Spectrometry. *J. Proteome Res.* **21**, 1789–1799 (20**22**).
24. Schmidlin, T. et al. High-Throughput Assessment of Kinome-wide Activation States. *Cell systems* **9**, 366-374.e5 (2019).
25. Keshishian, H. et al. A highly multiplexed quantitative phosphosite assay for biology and preclinical studies. *Mol Syst Biol* **17**, (2021).
26. Bentum, M. van & Selbach, M. An introduction to advanced targeted acquisition methods. *Mol Cell Proteomics* **20**, 100165 (2021).
27. Stopfer, L. E. et al. High-density, targeted monitoring of tyrosine phosphorylation reveals activated signaling networks in human tumors. *Cancer Res* canres.3804.2020 (2021) doi:10.1158/0008-5472.can-20-3804.
28. Martínez-Val, A. et al. Hybrid-DIA: intelligent data acquisition integrates targeted and discovery proteomics to analyze phospho-signaling in single spheroids. Nat. Commun. **14**, 3599 (2023).
29. Derks, J. et al. Increasing the throughput of sensitive proteomics by plexDIA. *Nat. Biotechnol.* **41**, **50**–59 (2023).
30. Thielert, M. et al. Robust dimethyl-based multiplex-DIA doubles single-cell proteome depth via a reference channel. Mol. Syst. Biol. 19, e11503 (2023).
31. Welter, A. S. et al. Combining data independent acquisition with spike-in SILAC (DIA-SiS) improves proteome coverage and quantification. (2024) doi:10.1101/2024.05.03.592381.
32. Gerber, S. A., Rush, J., Stemman, O., Kirschner, M. W. & Gygi, S. P. Absolute quantification of proteins and phosphoproteins from cell lysates by tandem MS. *Proc National Acad Sci* **100**, 69**40**–6945 (2003).
33. Gaither, C., Popp, R., Mohammed, Y. & Borchers, C. H. Determination of the concentration range for **26**7 proteins from 21 lots of commercial human plasma using highly multiplexed multiple reaction monitoring mass spectrometry. *Analyst* **145**, 3634–3644 (2020).
34. Lesur, A. et al. Quantification of 782 Plasma Peptides by Multiplexed Targeted Proteomics. J. Proteome Res. 22, 1630–1638 (2023).
35. Yu, Q. et al. Sample multiplexing for targeted pathway proteomics in aging mice. Proc National Acad Sci **117**, 9723–9732 (2020).
36. Ong, S.-E. et al. Stable Isotope Labeling by Amino Acids in Cell Culture, SILAC, as a Simple and Accurate Approach to Expression Proteomics*. Mol. Cell. Proteom. 1, 3**76**–386 (2002).
37. Cox, J. & Mann, M. MaxQuant enables high peptide identification rates, individualized p.p.b.-range mass accuracies and proteome-wide protein quantification. Nat. Biotechnol. 26, 1367–1372 (2008).
38. Tsherniak, A. et al. Defining a Cancer Dependency Map. Cell **170**, 564-576.e16 (2017).
39. Suehnholz, S. P. et al. Quantifying the Expanding Landscape of Clinical Actionability for Patients with Cancer. *Cancer Discov.* **14**, 49–65 (2023).
40. Parker, T. W. & Neufeld, K. L. APC controls Wnt-induced β-catenin destruction complex recruitment in human colonocytes. *Sci. Rep.* **10**, 2957 (2020).
41. Dérijard, B. et al. JNK1: A protein kinase stimulated by UV light and Ha-Ras that binds and phosphorylates the c-Jun activation domain. Cell 76, 1025–1037 (1994).
42. Nakano, R., Nakayama, T. & Sugiya, H. Biological Properties of JNK3 and Its Function in

Neurons, Astrocytes, Pancreatic β-*Cells* and Cardiovascular Cells. Cells **9**, **18**02 (2020).
43. Krug, K. et al. A Curated Resource for Phosphosite-specific Signature Analysis* [S]. Mol. Cell. Proteom. 18, 576–593 (2019).
44. Wiredja, D. D., Koyutürk, M. & Chance, M. R. The KSEA App: a web-based tool for kinase activity inference from quantitative phosphoproteomics. *Bioinformatics* **33**, 3489–3491 (2017).
45. Mischnik, M. et al. IKAP: A heuristic framework for inference of kinase activities from Phosphoproteomics data. Bioinformatics **32**, 424–431 (2016).
46. Mari, T. et al. In Vitro Kinase-to-Phosphosite Database (iKiP-DB) Predicts Kinase Activity in Phosphoproteomic Datasets. J. Proteome Res. 21, 1575–1587 (2022).
47. Yu, K., Toral-Barza, L., Shi, C., Zhang, W.-G. & Zask, A. Response and determinants of cancer cell susceptibility to PI3K inhibitors: Combined targeting of PI3K and Mek1 as an effective anticancer strategy. *Cancer Biol. Ther.* **7**, 310–318 (2008).
48. Haagensen, E. J., Kyle, S., Beale, G. S., Maxwell, R. J. & Newell, D. R. The synergistic interaction of MEK and PI3K inhibitors is modulated by mTOR inhibition. *Br. J. Cancer* **106**, 1386–1394 (2012).
49. Wee, S. et al. PI3K Pathway Activation Mediates Resistance to MEK Inhibitors in KRAS Mutant Cancers. *Cancer Res.* **69**, 4286–4293 (2009).
50. García-García, C. et al. MEK plus PI3K/mTORC1/2 Therapeutic Efficacy Is Impacted by TP53 Mutation in Preclinical Models of Colorectal Cancer. *Clin. Cancer Res.* **21**, 5499–5510 (2015).
51. Temraz, S., Mukherji, D. & Shamseddine, A. Dual Inhibition of MEK and PI3K Pathway in KRAS and BRAF Mutated Colorectal Cancers. *Int. J. Mol. Sci.* **16**, 22976–22988 (2015).
52. Chen, J. et al. A combinatorial strategy for overcoming primary and acquired resistance of MEK inhibition in colorectal cancer. *Exp. Cell Res.* **393**, 112060 (2020).
53. Searle, B. C. et al. A Multipathway Phosphopeptide Standard for Rapid Phosphoproteomics Assay Development. Mol. Cell. Proteom. 22, 100639 (2023).
54. Morkel, M., Riemer, P., Bläker, H. & Sers, C. Similar but different: distinct roles for KRAS and BRAF oncogenes in colorectal cancer development and therapy resistance. *Oncotarget* **6**, 20785–20800 (2015).
55. Klinger, B. & Blüthgen, N. Consequences of feedback in signal transduction for targeted therapies. *Biochem. Soc. Trans.* **42**, 770–5 (2014).
56. Koveitypour, Z. et al. Signaling pathways involved in colorectal cancer progression. *Cell Biosci.* **9**, 97 (2019).
57. Jeffrey, K. L., Camps, M., Rommel, C. & Mackay, C. R. Targeting dual-specificity phosphatases: manipulating MAP kinase signalling and immune responses. Nat. Rev. Drug Discov. 6, 391–403 (2007).
58. Schmid, C. A. et al. DUSP4 deficiency caused by promoter hypermethylation drives JNK signaling and tumor cell survival in diffuse large B cell lymphoma. *J. Exp. Med.* **212**, 775–792 (2015).
59. Xue, Z. et al. MAP3K1 and MAP2K4 mutations are associated with sensitivity to MEK inhibitors in multiple cancer models. Cell Res. **28**, 719–729 (2018).
60. Jansen, R. A. et al. Small-molecule inhibition of MAP2K4 is synergistic with RAS inhibitors in KRAS-mutant cancers. *Proc. Natl. Acad. Sci.* **121**, e2319492121 (2024).
61. Friedrich, C. et al. Comprehensive micro-scaled proteome and phosphoproteome characterization of archived retrospective cancer repositories. Nat. Commun. 12, 3576 (2021).
62. Mund, A. et al. Deep Visual Proteomics defines single-cell identity and heterogeneity.

Nat. Biotechnol. 40, 1231–1240 (2022).
63. Makhmut, A. et al. A framework for ultra-low-input spatial tissue proteomics. *Cell Syst.* **14**, 1002-1014.e5 (2023).
64. Mertins, P. et al. Reproducible workflow for multiplexed deep-scale proteome and phosphoproteome analysis of tumor tissues by liquid chromatography–mass spectrometry. *Nat Protoc* **13**, 1632–1661 (2018).
65. Ritchie, M. E. et al. limma powers differential expression analyses for RNA-sequencing and microarray studies. Nucleic Acids Res. 43, e47–e47 (2015).
66. Perez-Riverol, Y. et al. The PRIDE database resources in 2022: a hub for mass spectrometry-based proteomics evidences. Nucleic Acids Res. 50, D543–D552 (2021).